

# ADVANCED FUNCTIONAL MATERIALS

## Supporting Information

for *Adv. Funct. Mater.*, DOI: 10.1002/adfm.202008039

### Tunable, Grating-Gated, Graphene-On-Polyimide Terahertz Modulators

*Alessandra Di Gaspare, Eva Arianna Aurelia Pogna, Luca Salemi, Osman Balci, Alisson Ronieri Cadore, Sachin Maruti Shinde, Lianhe Li, Cinzia di Franco, Alexander Giles Davies, Edmund Harold Linfield, Andrea Carlo Ferrari, Gaetano Scamarcio, and Miriam Serena Vitiello\**

# Supporting Information

## Tunable, grating-gated graphene-on-polyimide terahertz modulators

Alessandra Di Gaspare<sup>1</sup>, Eva A.A. Pogna<sup>1</sup>, Luca Salemi<sup>1</sup> Osman Balci<sup>2</sup>, Alisson R. Cadore<sup>2</sup>, Sachin M. Shinde,<sup>2</sup> Lianhe Li,<sup>3</sup> Cinzia di Franco<sup>4</sup>, A. Giles Davies,<sup>3</sup> Edmund Linfield,<sup>3</sup> Andrea Ferrari<sup>2</sup>, Gaetano Scamarcio<sup>4</sup> and Miriam S. Vitiello<sup>1</sup>

<sup>1</sup>NEST, CNR-NANO and Scuola Normale Superiore, 56127 Pisa, Italy

<sup>2</sup>Cambridge Graphene Centre, Cambridge CB3 0FA, UK

<sup>3</sup>School of Electronic and Electrical Engineering, University of Leeds, Leeds LS2 9JT, UK

<sup>4</sup>CNR-IFN and Dipartimento Interateneo di Fisica, Università degli Studi di Bari, I-70126 Bari, Italy

### 1. Characterization of the SLG

Fig. S1a shows an optical microscopy image of SLG on the grating gate structure. As grown and transferred SLG samples (Fig. S1a) are characterized by Raman spectroscopy using Renishaw InVia spectrometer. The 514.5 nm spectrum of as grown SLG on Cu foil after Cu photoluminescence removal [1] is shown in Fig. S1b (blue spectrum).

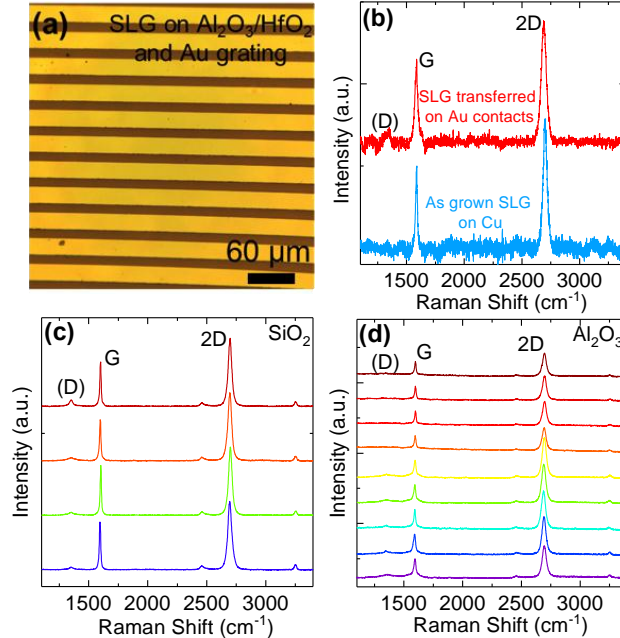


**Figure S1:** (a) Optical microscopy image of the grating gated SLG THz modulator after the SLG transfer. The yellow stripes are the Au electrodes (grating gate), and the brown stripes are the AlO<sub>x</sub>/HfO<sub>2</sub>/polyimide/Au/SiO<sub>2</sub>/Si regions. (b) Raman spectra at 514.5nm of as grown SLG on Cu (blue) and transferred SLG onto the Au contacts of our THz modulator (red). (c,d) Raman spectra at 514.5nm of SLG transferred on (c) SiO<sub>2</sub>, (d) Al<sub>2</sub>O<sub>3</sub>.

The 2D peak at  $\sim 2730 \text{ cm}^{-1}$  is a single Lorentzian with  $\text{FWHM}(2D) \sim 28 \text{ cm}^{-1}$ , signature of SLG [2]. The G peak at  $\text{Pos}(G) \sim 1584 \text{ cm}^{-1}$  has  $\text{FWHM}(G) \sim 15 \text{ cm}^{-1}$ . The intensity and area ratios of 2D and G peak are  $I(2D)/I(G) \sim 1.6$  and  $A(2D)/A(G) \sim 3$ . The ratio of D and G Peak intensities indicates a negligible defect density in as grown SLG [3,4]. The 514.5 nm Raman spectrum of the transferred SLG on the Au contacts of our THz modulator is shown in Fig. S1b (red spectrum). In this case,  $\text{Pos}(G) \sim 1584 \text{ cm}^{-1}$ ,  $\text{FWHM}(G) \sim 27 \text{ cm}^{-1}$ ,  $\text{Pos}(2D) \sim 2690 \text{ cm}^{-1}$ ,  $\text{FWHM}(2D) \sim 45 \text{ cm}^{-1}$ ,  $I(2D)/I(G) \sim 1.6$ ,  $A(2D)/A(G) \sim 2.6$ ,  $I(D)/I(G) \sim 0.09$ . To estimate  $E_F$  and defect density after transfer, we measure Raman spectra of the transferred SLG on SiO<sub>2</sub> (Fig.S1c) and atomic layer deposition (ALD) grown Al<sub>2</sub>O<sub>3</sub> (Fig. S1d). On SiO<sub>2</sub>, the average Raman fitting parameters and standard deviations over a broad set of measurements on several samples are:  $\text{Pos}(G) \sim 1598 \pm 3 \text{ cm}^{-1}$ ,  $\text{FWHM}(G) \sim 12.8 \pm 1.0 \text{ cm}^{-1}$ ,  $\text{Pos}(2D) \sim 2697 \pm 2 \text{ cm}^{-1}$  and mean  $\text{FWHM}(2D) \sim 34.1 \pm 2.1 \text{ cm}^{-1}$ ,  $I(2D)/I(G) \sim 1.5 \pm 0.1$ ,  $A(2D)/A(G) \sim 4.1 \pm 0.2$ . These indicate  $E_F \sim 0.23 \pm 0.11 \text{ eV}$ , with p-type doping [5,6].  $I(D)/I(G) \sim 0.08 \pm 0.04$  indicates  $\sim 1.9 \pm 1 \times 10^{10} \text{ cm}^{-2}$  defect density [3,4]. On Al<sub>2</sub>O<sub>3</sub>, the average Raman fitting parameters and standard deviations over a broad set of measurements on several samples give:  $\text{Pos}(G) \sim 1595 \pm 3 \text{ cm}^{-1}$ ,  $\text{FWHM}(G) \sim 18.8 \pm 4.1 \text{ cm}^{-1}$ ,  $\text{Pos}(2D) \sim 2694 \pm 3 \text{ cm}^{-1}$ ,  $\text{FWHM}(2D) \sim 39.1 \pm 1.4 \text{ cm}^{-1}$ ,  $I(2D)/I(G) \sim 2.1 \pm 0.3$ ,  $A(2D)/A(G) \sim 4.5 \pm 0.7$ . This indicates  $E_F \sim 0.23 \pm 0.11 \text{ eV}$ , p-type [5,6].  $I(D)/I(G) \sim 0.06 \pm 0.06$  indicates  $\sim 1.5 \pm 1.5 \times 10^{10} \text{ cm}^{-2}$  defect density [3,4].

## 2. Time Domain Spectroscopy

The reflectivity of the SLG THz modulator is measured via time domain spectroscopy (Menlo System Terasmart k5) (Figs. S1a-b.) The beam spot diameter in reflection mode is 1.5 mm, resulting in a beam area smaller than the active area of the modulators. The time-domain THz signal is acquired with a delayed-pulse sampling window of  $\sim 70 \text{ ps}$ , resulting in a spectral resolution  $\sim 15 \text{ GHz}$ . A prototypical pulse acquisition, for the SLG modulator with  $p = 10 \text{ }\mu\text{m}$  and at  $V_G = 0 \text{ V}$ , is shown in Fig. S2c. The time-traces are recorded in a N<sub>2</sub> purged environment with the modulator positioned in the focus of the optical path. The black curve, in Fig. S2c, retrieved from the Au surface corresponds the THz pulse emitted by the photoconductive antenna transmitter module, used as a reference for the extraction of the reflectivity and of the spectral power of the incoming beam. The corresponding spectral distribution (Fig. S2d) is obtained upon Fourier transforming the time-domain of Fig S2c traces.

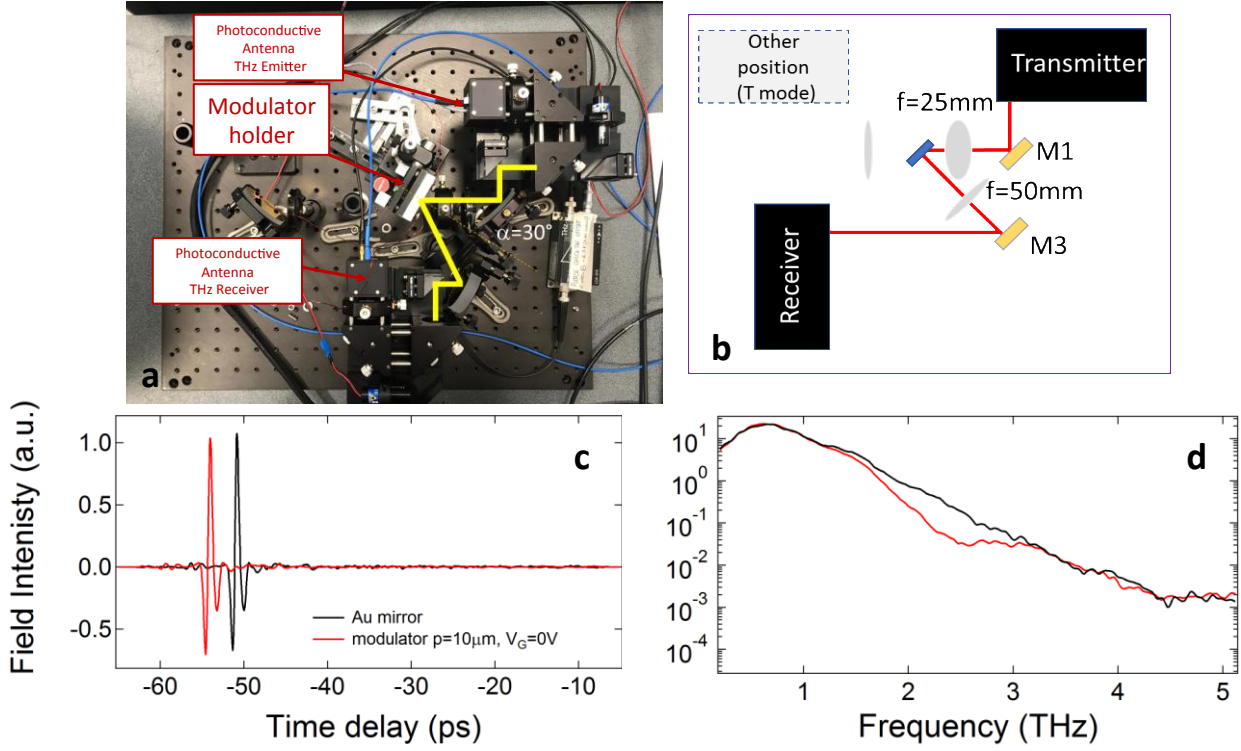


**Figure S2:** (a) TDS system (Terasmart k5) used for R characterization of the modulators. The yellow line represents the beam optical path. (b) Schematic layout of optical path for TDS reflection mode operation, employing two 2" diameter TPX lenses with focal lengths  $f = 25\text{mm}$  for the focusing of the incoming beam on the sample (spot diameter on the sample  $\sim 1.5\text{mm}$ ), and  $50\text{mm}$  for the collection of the reflected beam. (c) Time-trace of the reflected electric field from a reference plane Au mirror (black curve) and from the modulator (red curve) with  $p = 10\ \mu\text{m}$  in the TDS setup shown in panel a. (d) Spectral distribution of the reflected electric fields calculated through Fourier transform of the time-traces in panel (c).

### 3. Graphene optical conductivity

The conductivity of SLG is depends on two fundamental electronic transitions: interband and intraband [7-10]. The interband conductivity due to the interband transitions in SLG can be approximated as [7]:

$$\sigma_{inter}(\omega) = \frac{e}{4\hbar} \left[ H\left(\frac{\omega}{2}\right) + \frac{4i\omega}{\pi} \int_0^{\omega} d\omega' \frac{H(\omega') - H(\frac{\omega}{2})}{\omega^2 - 4\omega'^2} \right] \quad (S1)$$

$$H(\omega') = \frac{\sinh\left(\frac{\hbar\omega'}{k_B T}\right)}{\cosh\left(\frac{E_F}{k_B T}\right) + \cosh\left(\frac{\hbar\omega'}{k_B T}\right)}$$

and where  $k_B$  is the Boltzmann constant,  $T$  is the temperature,  $\omega$  is the frequency of light. At THz frequencies, intraband electronic transitions dominate the conductivity of SLG due to the fact that even at moderate  $E_F$  ( $\sim 20\text{meV}$ ) interband transitions are blocked.

SLG then behaves as a two-dimensional electron gas, with a Drude-like conductivity (called intraband conductivity) [7,8,10]:

$$\sigma_{intra}(\omega) \sim \sigma_{Drude}(\omega) = \sigma_{DC} \frac{1}{1 - i\omega\tau} \quad (S2)$$

Where  $\sigma_{DC}$  is the DC conductivity of SLG as  $\omega \rightarrow 0$  and  $\tau$  is the scattering time. The DC conductivity can be written as  $\sigma_{DC} = \frac{2e^2}{h} |k_F| v_F \tau$ , where  $k_F = \sqrt{\pi n}$ ,  $v_F \sim 1.1 \times 10^5$  m/s is Fermi velocity. The total optical conductivity of SLG can be written as the sum of interband and intraband components as [7,8,10];

$$\sigma_{SLG}(\omega) = \sigma_{intra}(\omega) + \sigma_{inter}(\omega) \quad (S3)$$

$\sigma_{SLG}(\omega)$  is plotted in Fig.S3. In FIR and THz, it is mostly dominated by intraband transitions and the contributions from interband transitions are negligible. In our simulations in COMSOL, we neglect the interband contribution and we only use the Drude-like conductivity originating from intraband transitions, since our SLG has  $E_F \sim 200$  meV, as extracted from Raman experiments.

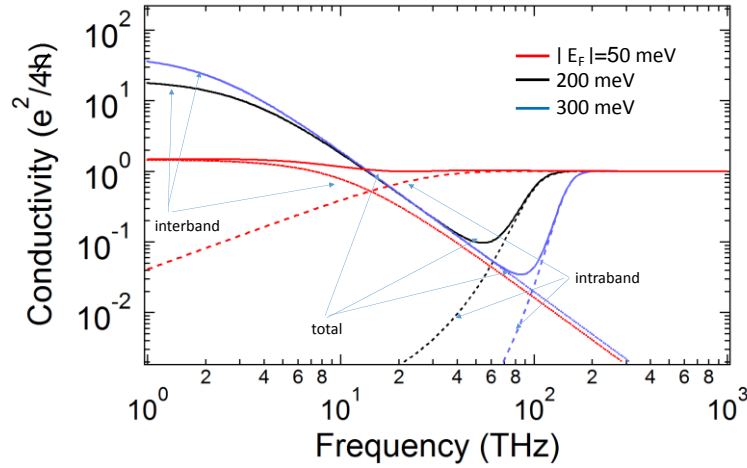


**Figure S3:**  $\sigma_{SLG}(\omega)$  in units of universal conductance  $G_0 = e^2/4h = 6.08 \times 10^{-5}$  S, for  $E_F = 50$  meV (red), 200 meV (black) and 300 meV (blue). For each curve, the  $E_F$  dependent scattering time is calculated as  $\tau = \mu E_F / e v_F$ , by assuming  $\mu \sim 1600 \text{ cm}^2/\text{Vs}$  (as extracted from the transfer characteristics of a SLG field effect transistor). The intraband (Drude) and interband terms are shown separately

#### 4. Electrostatic simulation of graphene-Au grating capacitor

Our SLG THz modulators use an Au grating as the gate electrode with a  $\text{AlOx}/\text{HfO}_2$  dielectric layer on top. SLG is placed on the dielectric layer to form the SLG-Au grating capacitor. The voltage difference applied between SLG and Au grating creates a constant and uniform electric field between the electrodes. However, the electric field intensity decays in the proximity of the Au grating and creates a non-uniform fringing electric field distribution on the SLG. In order to verify the DC electric field distribution on SLG, we perform finite element simulations by using the AC/DC module in COMSOL Multiphysics.

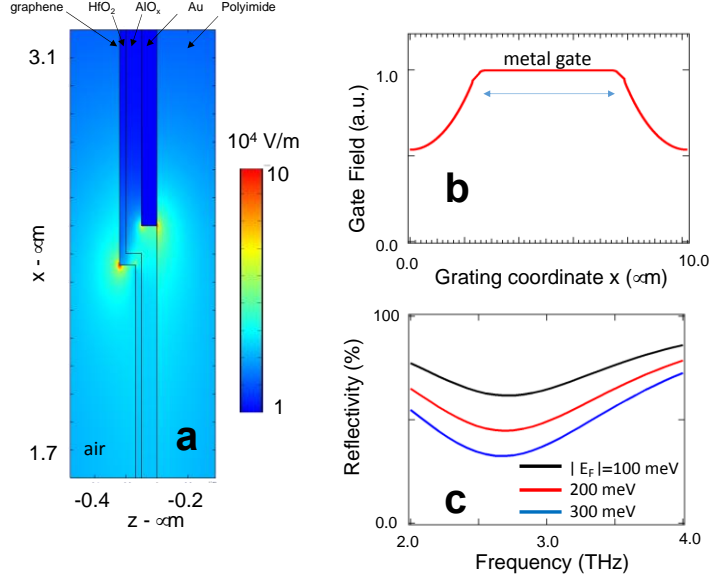


**Figure S4:** (a) Bi-dimensional static electric field distribution (b) Electric field profile from simulation of panel (a) in close proximity of SLG (5 nm) for  $p = 10 \mu\text{m}$ ,  $V_G = 10\text{V}$ . (c) Reflectivity modulation from static electric field distribution in (a-b).

We model the dielectric layers by assuming a gate resistance of  $\sim 3 \text{ M}\Omega$  for the AlO<sub>x</sub> layer, and  $\sim 1 \text{ G}\Omega$  for the HfO<sub>2</sub> layer; these values are extracted from direct IV measure of the gate dielectric current on the as-grown films realized ad-hoc. We apply 10V to the Au grating and calculate the static electric field distribution in proximity of the SLG. Fig.S4a is the color map for the calculated static electric field distribution along the Au grating coordinate (x-axes in Fig. s4a). The static electric field variation, calculated in close proximity of the SLG along the Au grating direction is in Fig.S4b. The field is constant below the grating, then decays at both edges and it saturates at half intensity of the top field below the grating. This forms a finite electric field distribution on SLG. We then use this static electric field profile to set the SLG  $E_F$  to simulate the performance of the SLG THz modulators. We model SLG as a transient boundary condition with  $\sigma_{DC} = e^2 \tau E_f / \pi \hbar^2$ . We set  $E_F = 100 - 300 \text{ meV}$  in the gated region (flat profile), and the scattering time  $\tau = \mu E_F / e v_F$ , by assuming a mobility  $\mu \sim 1600 \text{ cm}^2/\text{Vs}$ . The reflectivity modulation for  $p = 10 \mu\text{m}$  is shown in Fig. S4c. The chosen  $E_F$  correspond to  $V_G$  used in our experiments (Figs 2). We retrieve a reflectivity modulation (Fig. 4Sc) in agreement with the experiments in Figs. 2.

## 5. Graphene Field Effect Transistors Parameters

The  $E_F$  values used in the EMW simulations are chosen to reproduce the experimentally measured reflectivity curves of Figs 2. To estimate the  $E_F$  shift on SLG with  $V_G$ , we fabricate a SLG field effect transistor (GFET) using the same dielectric configuration and thicknesses as those used in the SLG modulators, but grown on doped GaAs. We transfer SLG on AlOx/HfO<sub>2</sub> and fabricate Cr(10nm)/Au(100 nm) contact pads on SLG. The SLG is shaped by O<sub>2</sub> plasma to define the GFET channel with width=60 μm and length=60μm. A schematic drawing of the GFET side view is in Fig. S5a.

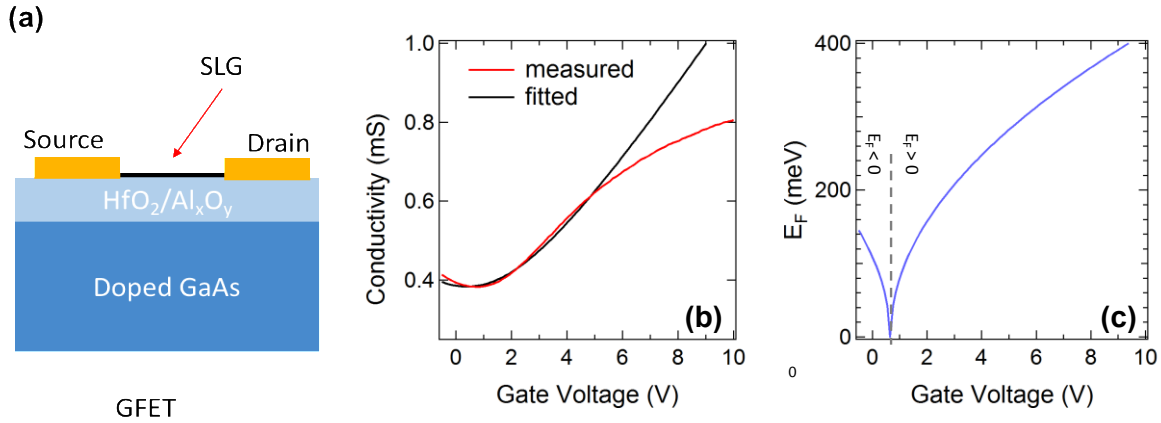


**Figure S5:** (a) Schematic back gate GFET on a doped GaAs with AlOx/HfO<sub>2</sub> gate dielectric. (b) Measured conductivity of the GFET with Drude model fitting to estimate  $n_0$  and  $\mu$ . (c) Estimated  $E_F$  change with  $V_G$ .

We first measure the transfer characteristics of the GFET as a function of  $V_G$  with drain voltage of 3 mV. We estimate the SLG conductivity, Fig. S5b, by subtracting the contact resistance  $R_C=410 \Omega$  extracted from the IV curve from the measured total resistance. From the Drude model, the  $V_G$  dependent conductivity of SLG is [8,9]:

$$\sigma(V_G) = \mu e n_{Tot}(V_G) = \mu e \sqrt{n_0^2 + n^2(V_G)} = \mu e \sqrt{n_0^2 + \left(\frac{C_{ox}}{e}\right)^2 (V_G - V_{CNP})^2} \quad (S4)$$

where  $\mu$  is the charge carrier mobility,  $e$  is the electronic charge,  $n_0$  is the residual charge density,  $n(V_G)$  is the gate dependent charge density of graphene,  $C_{ox}$  is the gate oxide capacitance,  $V_{CNP}$  is the charge neutrality point voltage. In our sample,  $V_{CNP} = +0.7$  V and the SLG was initially p-doped. To fit the measured conductivity, we used  $n_0 \sim 1.57 \times 10^{12} \text{cm}^{-2}$  and estimate  $\mu \sim 1550 \text{cm}^2/\text{Vs}$ . We then calculate  $E_F = \hbar v_F \sqrt{\pi n(V_G)}$ . The defined Fermi energy is estimated as  $E_F \sim -110 \text{meV}$  and it goes up to  $E_F \sim +400 \text{meV}$  with  $V_G$ , Fig.S5c.

## 6. Modulator Insertion Losses

To calculate the total insertion losses  $\delta^{\text{dB}}$  of the modulator we use the following equation [11]:

$$\delta^{\text{dB}} = -10 \log \frac{P_{\text{mod},r}}{P_{\text{Au},r}} \quad (\text{S5})$$

where  $P_{\text{mod},r}$  is the total power reflected by the modulator (output power), and  $P_{\text{Au},r}$  is the total power measured with the reference Au mirror positioned in the focus of the optical path (input power).

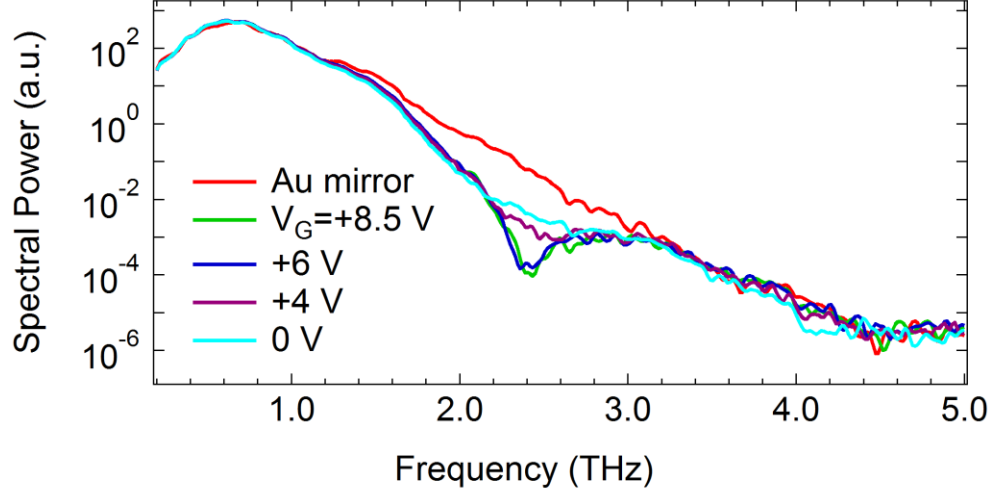


**Figure S6:** Spectral power distribution calculated from Fourier-transform of the square-amplitude of the electric field timetraces measured through TDS from the Au plane mirror and from the modulator with  $p = 10 \mu\text{m}$ , at different  $V_G$ .

To calculate the total power, we integrate the spectral power retrieved from the time domain spectroscopy data over the optical bandwidth (OB) of interest.

$$P_{\text{mod},r} = \int_{\text{OB}} d\nu P_{\text{mod},r}^{\nu} \quad (\text{S6})$$

and

$$P_{\text{Au},r} = \int_{\text{OB}} d\nu P_{\text{Au},r}^{\nu} \quad (\text{S7})$$

where  $P_{\text{mod},r}^{\nu}$  and  $P_{\text{Au},r}^{\nu}$  are the spectral powers of modulator and of reference gold-mirror, respectively. Their values are calculated from Fourier transformation of the corresponding square-amplitude electric-fields measured via time domain spectroscopy over an optical bandwidth of 1-4 THz. Fig.S6 shows the spectral power retrieved for the modulator with  $p = 10 \mu\text{m}$  and for the reference Au mirror. We obtain  $\delta^{\text{dB}} = 0.7 \text{ dB}$  for  $V_G = -10\text{V}$  and  $\delta^{\text{dB}} = 1.3 \text{ dB}$  for  $V_G = +10\text{V}$ .

## 7. Gate voltage dependence of the intermode beatnote linewidth in QCL

To investigate the role of  $V_G$  on the intracavity dynamics of the QCL comb, we compare the intermode beatnote map at three distinctive  $V_G$  values with the SLG modulator with  $p=10 \mu\text{m}$ . The comparison between the intermode beatnote linewidths (Fig. S7), in two relevant current ranges (400-650 mA and 760-820 mA) in which the modulator-coupled QCL operates as a stable comb, unveils that the reflectivity modulation  $V_G = 0$  is sufficient to compensate the intracavity dispersion and that larger  $V_G$  do not induce visible changes on the QCL comb behavior, in agreement with simulations of Fig. 4.

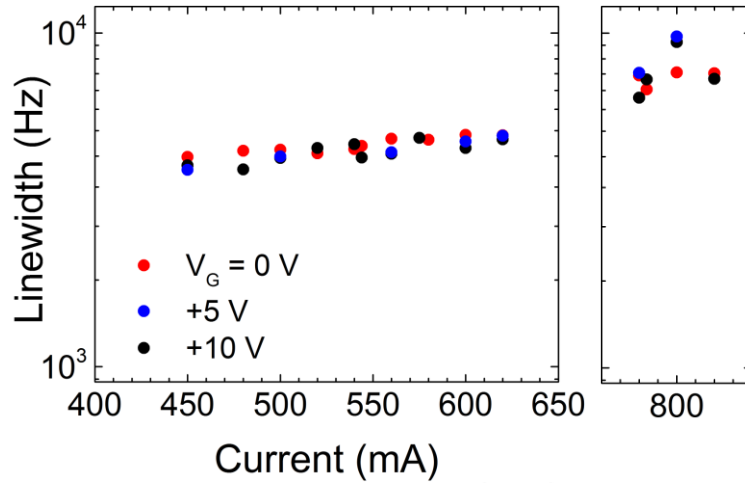


**Figure S7:** Evolution of intermode beatnote linewidths as a function of QCL driving current when the QCL is coupled with the SLG modulator with  $p=10 \mu\text{m}$ ,  $V_G=0\text{V}$  (red dots),  $+5\text{V}$  (blue) and  $+10\text{V}$  (black). The linewidths are reported for the two FC operation regions with narrow and individual beatnote. (a) bias current 400-620 mA and (b) 780-820 mA.

## 7. Comparison between the intermode beatnote maps

Figure S8 shows the comparison between the intermode beatnote maps retrieved in the bare QCL or while coupling the QCL with the SLG modulator having  $p = 10 \mu\text{m}$ .

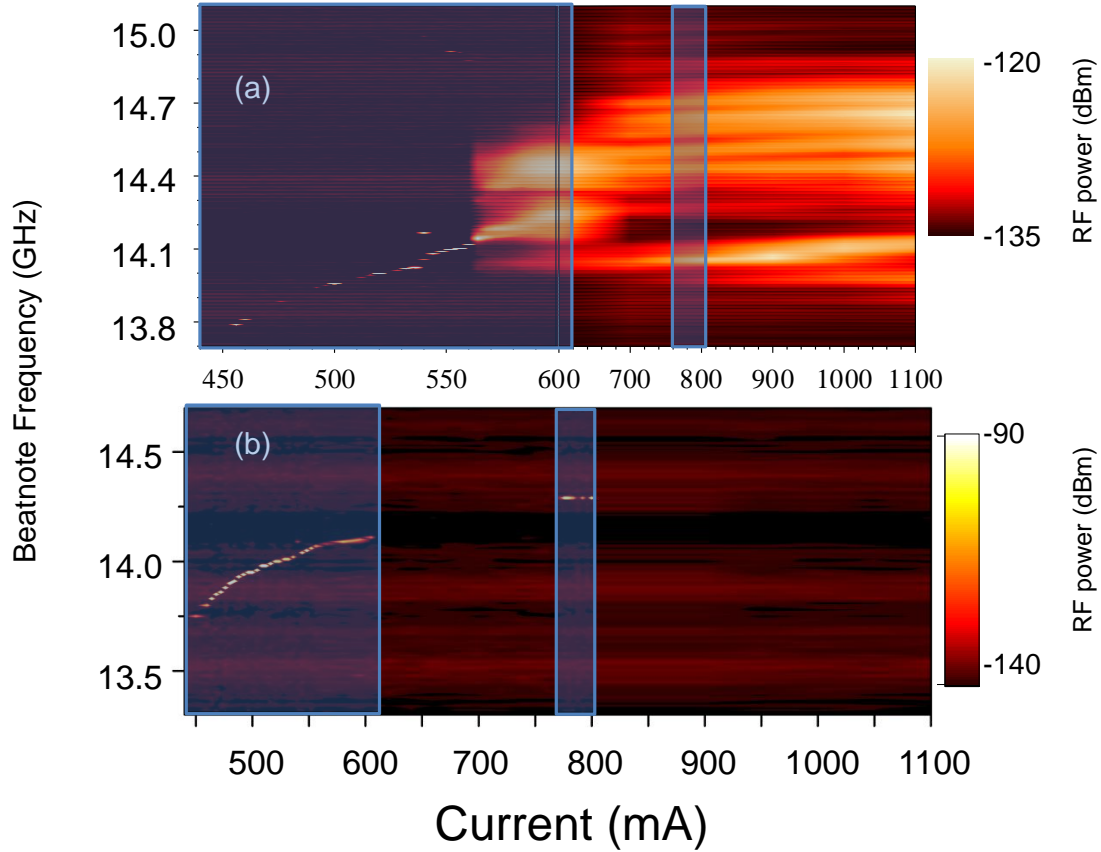


**Figure S8** Intermode beatnote maps as a function of CW driving current measured at 15 K in the bare QCL **(a)** and QCL-modulator system with  $p = 10 \mu\text{m}$  **(b)**. The shaded light-blue rectangles show the range of currents in which the SLG-coupled QCL behaves as a frequency comb. The beat-note signal is extracted from the bias line using a bias-tee with a RF spectrum analyzer, and is recorded with resolution bandwidth (RBW): 500 Hz, video bandwidth (VBW): 500 Hz, sweep time (SWT): 20 ms, RMS (root mean square) acquisition mode.

## References

1. Lagatsky, A. A., et al. 2  $\mu\text{m}$  solid-state laser mode-locked by single-layer graphene. *App. Phys. Lett.*, **102**, (2013)
2. Ferrari, A. C., et al. Raman Spectrum of Graphene and Graphene Layers. *Phys. Rev. Lett.*, **97**, 187401 (2006)
3. Cançado, L. G., et al. Quantifying Defects in Graphene via Raman Spectroscopy at Different Excitation Energies. *Nano Lett*, **11**, 3190 (2011)
4. Bruna, M., Ott, A. K., Ijäs, M., Yoon, D., Sassi, U., Ferrari, A. C. Doping Dependence of the Raman Spectrum of Defected Graphene. *ACS Nano*, **8**, 7432 (2014).
5. Basko, D. M., Piscanec, S., & Ferrari, A. C. Electron-electron interactions and doping dependence of the two-phonon Raman intensity in graphene. *Phys. Rev. B*, **80**, 165413, (2009).
6. Das, A., Pisana, S., Chakraborty, B. et al. Monitoring dopants by Raman scattering in an electrochemically top-gated graphene transistor. *Nat. Nanotech* **3**, 210 (2008)
7. Stauber, T., Peres, N. M. R., Geim A. K. Optical conductivity of graphene in the visible region of the spectrum. *Phys. Rev. B* **78**, 085432 (2008)
8. Docherty C. J. et al. Terahertz Properties of Graphene. *J Infrared Milli Terahz Waves* **33**, 797–815 (2012)

9. Nair R.R. et al. Fine Structure Constant Defines Visual Transparency of Graphene. *Science* **320**, 1308 (2008)
10. Sun, Z., Martinez, A., Wang, F. Optical modulators with 2D layered materials. *Nat. Phot.*, **10**, 227 (2016)
11. Bhattacharya, P.K, Semiconductor Optoelectronic Devices. ISBN 13: 9780134956565. Prentice Hall, (1996)